TEST, DIAGNOSTICS AND COMPUTED TOMOGRAPHIC INSPECTION OF A LARGE GRAIN 3.9 GHz PROTOTYPE CAVITY

M. Bertucci†, A. Bignami, A. Bosotti, J.F. Chen, C. G. Maiano, P. Michelato, L. Monaco, R. Paparella, P. Pierini*, D. Sertore, INFN–LASA, Segrate (MI), Italy
G. Ciovati, G. R. Myneni, JLab, Newport News, Virginia, USA
C. Pagani, University of Milano & INFN-LASA, Milano, Italy

Abstract

A large grain 3.9 GHz prototype cavity made of RRR = 105 +/-10 has been tested at LASA. The cavity suffered of quench at moderate levels of accelerating field, for all nine fundamental pass-band modes. Several diagnostic techniques have been employed to determine the quench positions, which occur close to significant grain-boundary steps, visible from the external cavity surface. The cavity has been scanned with a high resolution X-ray tomographic machine, confirming the existence of remarkable topographic features on the inner RF surface at the suspected quench positions. A strategy for a future surface treatment for recover the cavity performances is here presented.

INTRODUCTION

In parallel with the work for the realization of the 3rd harmonic 3.9 GHz XFEL injector, LASA-INFN has conducted a non-in kind R&D activity on large grain niobium material. The material, supplied to LASA by Jefferson Lab (JLab, USA), is produced by CBMM, Brasil. From measurement on samples extracted from ingot, a RRR=100 is obtained with a Ta content of 1375 ppm wt. The same material has been employed by JLab for the fabrication of a 1.5 GHz single cell cavity which achieved reproducibly a peak magnetic field of 90 mT (about 20 MV/m) and Q values of the order of 2×10^{10} at 2K [1]. A prototype cavity has been therefore realized by LASA exploiting the same mechanical design and the same treatment cycle of 3.9 GHz XFEL cavities [2], so to have a prompt feedback of LG material performance by comparing it with the results of series production tests.

CAVITY TEST RESULTS

The LG 3.9 GHz prototype cavity (3HZLG) has been tested at LASA. Fig.1 shows the results for the π mode power rise at 1.8 and 2 K. The cavity quenched barely above 10 MV/m at 2K, without exhibiting any significant Q-slope, clearly showing a worse performance than the series production cavities. No radiation is detected from external proportional counter.

The 9 passband modes have also been measured. The reconstructed mode profiles at quench field are reported in table 1. The cavity is able to locally reach the gradient of 18/19 MV/m, comparable to gradients achieved in 3.9 GHz XFEL series production, so that one can state that no global mechanism of dissipation is limiting the cavity performance. Furthermore, the quench field increased to 10.9 MV/m with Q_0 equal to 2.5×10^9 at 1.8K.

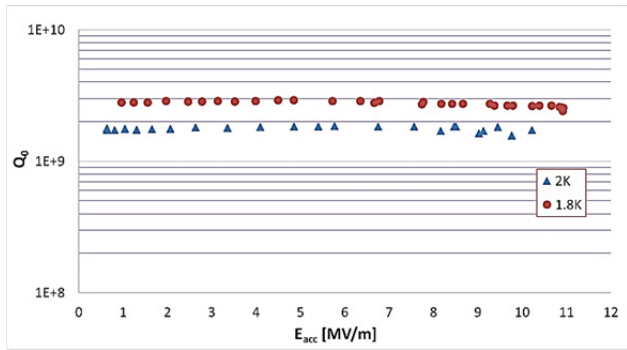

Figure 1: 3HZLG Q vs E_{acc} (π mode).

Table 1: cavity field profile in the 9 pass-band modes at quench field. Highlighted are the quench field values

# Cell	Fundamental pass band mode								
	π/9	2 π/9	3 π/9	4 π/9	5π/9	6 π/9	7 π/9	8 π/9	π
1-9	3	5	6	7	10	**15**	**17**	**11**	**10**
2-8	10	11	**11**	10	7	0	9	9	**10**
3-7	15	**13**	6	4	12	**15**	3	7	**10**
4-6	18	8	6	**11**	2	**15**	14	4	**10**
5	**19**	0	**11**	0	**13**	0	**18**	0	**10**
E_{max} MV/m	19	13	11	7	10	15	17	11	10

Quench Analysis

10 OST sensors [3] have been installed in a frame surrounding cavity external surface for second sound acquisition. In each pass-band mode test, a clear confined zone has been identified as quench site on cavity surface. On the whole, 4 families of quenching points are identified. Table 2 summarizes the quench localization on cavity surfaces for the 9 modes. The results of second sound agree with modal analysis, except for modes 3,4 and 5π/9, where significant discrepancy in the quench field occurs, as it ranges from 6 to 10 MV/m. The cell localization is moreover not congruent with modal analysis, since the higher field of 17 MV/m is reached in the 7 π/9 mode. In this case, however, the second sound trilateration algorithm provided a low precision (more than 1 cm).

* now at ESS, Lund
† michele.bertucci@mi.infn.it

ISBN 978-3-95450-182-3

Table 2: quench position as reconstructed by second sound on the 9 pass-band modes. “u” and “d” indicates if the point is displaced toward i-1 or i+1 cell, respectively

mode	E quench cell	quench position
π/9	15	eq. 3d 90°
2 π /9	13	eq. 3d 90°
3 π /9	6	eq. 1d 150°
4 π /9	7	eq. 1d 150°
5 π /9	10	eq. 1d 150°
6 π /9	15	eq. 3d 90°
7 π /9	18	eq. 5u 200°
8 π /9	9	eq. 8d 315°
π	10	eq. 8d 315°

Figure 2 shows the second sound reconstruction of the quench position for π mode. The breakdown event comes from 8-th cell equator, slightly displaced towards cell 7. The trilateration algorithm returned in this case a few mm precision for the quench position.

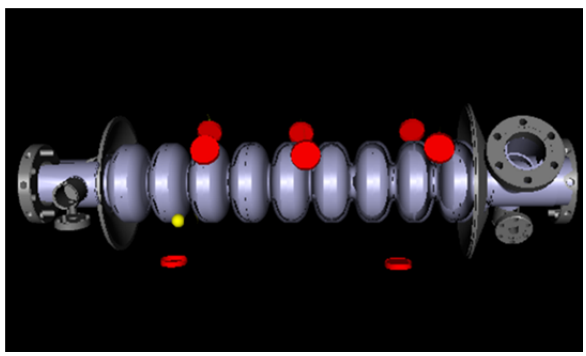

Figure 2: Second sound reconstruction of quench point (yellow dot). The red circles indicate the location of the OSTs.

Optical Inspection

An optical inspection of the inner cavity surface was performed in the equatorial and iris zone of each cell by means of a rigid borescope system after bulk BCP etching and 800 °C heat treatment [4] prior to final preparation for RF test.

Figure 3 shows the snapshot corresponding to quench position, acquired with a 27 μm/pixel optical resolution.

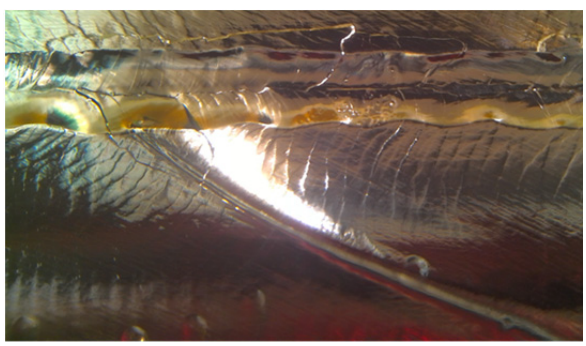

Figure 3: optical image at quench position, enlightening a grain boundary structure.

In the image, a grain boundary (GB) structure, beginning at heat affected zone and diagonally displacing toward iris, is evident. GB are known to be zones of preferential flux penetration due to local decrease of surface free energy [5] and are also suspected to be responsible of premature thermal breakdown due to magnetic field enhancement [3].

CAVITY 3D TOMOGRAPHY

Aiming to fully reconstruct GB topography, we performed a 3D X-ray computed tomography (CT) of the cavity. Due to high X-ray absorption cross section of niobium, ordinary tomographic machines characteristics does not allow a precise reconstruction of cavity inner geometry. We choose to use the YXLON CT Modular system, available at Agiometrix, in Bologna (Italy), which is nowadays the most powerful CT system available in Italy exploiting ordinary X-ray tubes. The X ray source operates up to 600 kV and 1.5 kW voltage and power with a focal spot of about 1 mm, therefore granting high penetration power with a maximum resolution of 24 μm voxel size [6].

Figure 4 shows a longitudinal section of inner cavity surface, as it is reconstructed by CT processing software. Except for iris regions, where bigger thickness and shadowing effects distort partially the 3D reconstruction algorithm, a clean rendering of surface topology is obtained. The blow-up in the box corresponds to the position of quench defect for mode π, as shown previously in fig. 3: a grain boundary structure can be definitively considered responsible of cavity quench at 10 MV/m.

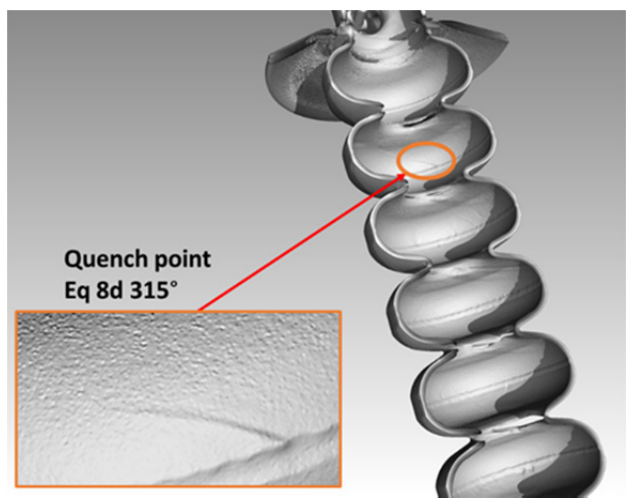

Figure 4: longitudinal section of cavity inner surface CT reconstruction. In the box, the detail of GB at quench point.

In order to evaluate GB profile depth, the 3D cavity volume is sliced horizontally in correspondence with grain boundary, slightly above the welding zone. Fig.5 shows a detail of GB section, with some characteristic sizes. At first glance, it can be noticed that GB zone is more than 0.4 mm re-entrant with respect to external surface.

Other defects found at quench location in other modes were also identified by 3D CT reconstruction. A report on the whole inner surface analysis performed with CT will be published in a future work.

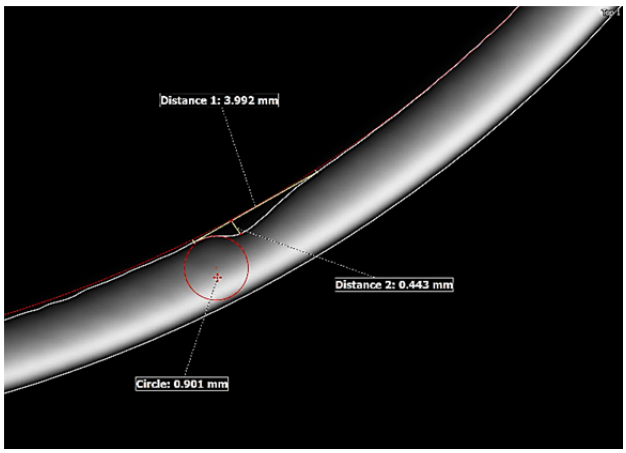

Figure 5: Cavity 2D slice at GB position (eq.8, slightly above welding), with some significant sizes.

DISCUSSION

Once a GB has been definitively identified as quench source from a qualitative point of view, it has still to be clarified which physical mechanism is involved. Several models have been proposed and studied [7, 8] to understand the role of GBs on cavity quench; amongst them impurity segregation, preferential flux penetration, and magnetic field enhancement.

The remarkable topology of defect leads us to pursue the trail of field enhancement, that can be handled from a quantitative point of view by a simple analytical model. Resorting to conformal map method developed by Kubo [9], it is possible to describe the GB defect in fig. 5 as a triangular pit with rounded edges. Due to irregular surface, local magnetic field can be expressed as $H(\vec{r}) = \beta(\vec{r})H_0$, where H_0 is the surface magnetic field in its turn depending on cavity E_{acc} and $\beta(\vec{r})$ is the magnetic field enhancement factor, depending on local shape. The maximum value for β can be obtained with the formula:

$$\beta_{max} = P(\gamma)\left(\frac{R}{r_e}\right)^{\gamma} \quad (1)$$

Where $2R$ is pit width, r_e the edge curvature radius, and $\gamma = \alpha/(1+\alpha)$ where $\pi\alpha$ is the wall angle. $P(\gamma)$ is a polynomial function of γ whose full expression can be found in the reference.

According to data taken from fig. 5, $2R = 3.99$ mm, $r_e = 0.90$ mm and $\alpha = 0.29$. Eq.1 gives a β_{max}=1.45 field enhancement factor. The corresponding quench field is $E^* = \beta_{max}E_{max} = 1.45 \cdot 10.2$=14.8 MV/m. We are still far from expected quench field of 20 MV/m but it has been nevertheless pointed out that defect geometry enhances noticeably the local peak field. Moreover, the discrepancy can be explained by comparing the characteristics of the two materials. Regardless of quench cause, the maximum magnetic can be calculated according to a simple thermal model [10] as:

$$H_{max} = \sqrt{\frac{4k(T_c - T_b)}{aR_n}} \quad (2)$$

Where a and R_n are defect size and surface resistance, T_c and T_b are niobium critical temperature (9.2K) and bath temperature (2K), and k is thermal conductivity. So the maximum field is proportional to square root of thermal conductivity. FG niobium employed for 3rd harmonic series production has RRR>300, at least 3 times greater than LG RRR=105. We can assume $k = RRR/4 = 75\ W/m \cdot K$ for FG material, but the same cannot be done for LG due to presence of phonon peak at 2K, whose height is very sensitive to mechanical crystal strain[11, 12]. According to previous reference, stress release after 800°C heat treatment yields a conductivity ratio $k_{2K}/k_{3K} = 1.65$ for $RRR{\sim}140$ LG material. An approximated value for $k = 1.65 * RRR/4 = 41\ W/m \cdot K$ can be therefore assumed for LG material. According to eq.1, $E_{max} \propto H_{max} \propto \sqrt{k}$, so that quench field for FG material should be higher by a $\sqrt{75/41} = 1.35$ factor with respect to LG. Multiplying this number with the value obtained by eq.1 we obtain 19.9 MV/m, which is very close to series production average maximum gradient [2]. These considerations, joined together, can explain the low field thermal breakdown of LG cavity.

CONCLUSIONS

RF measurement, diagnostics and analysis of 3.9 GHz large grain prototype cavity are here described. Second sound, cross checked with optical inspection, showed evidence of a grain boundary structure as responsible for cavity thermal breakdown at 10 MV/m. The subsequent x-ray tomographic inspection definitively confirmed this, moreover allowing a 3D evaluation of defect geometry. A magneto-thermal breakdown at the grain boundary is proposed as plausible hypothesis to explain the low quench field. In the follow-up, we propose to recover the cavity performance by means of 1) a local grinding of defective grain boundaries so to mitigate field enhancement and 2) a 1000°C annealing so to further increase thermal conductivity thanks to phonon peak recovery.

REFERENCES

[1] P. Dhakal *et al.,* "Effect of high temperature high treatments on the quality factor of a large-grain superconducting radio-frequency niobium cavity*", Phys. Rev. Accel. Beams,* vol. 16, p.042001, 2013.

[2] P. Pierini *et al.*, "Fabrication and vertical test experience of the European X-ray Free Electron Laser 3.9 GHz superconducting cavities", *Phys. Rev. Accel. Beams,* vol. 20, p.042006, 2017.

[3] R.A. Sherlock, D. O. Edwards, "Oscillating Superleak second sound transducers", *Rev. Sci. Instrum.*, vol. 41, p.1603, 1970.

[4] M. Bertucci, *Proc. SRF '13*, pp. 704-707.

ISBN 978-3-95450-182-3

[5] T. Matsushita, *Flux pinning in superconductors*, Springer, Berlin, 2007.

[6] Agiometrix, https://www.agiometrix.com/

[7] C. Z. Antoine, *Proc. CAS '13,* pp.209-245.

[8] V. Shemelin and H. Padamsee, TTC report SRF 080903-04.

[9] T. Kubo, in *Proc. SRF '13*, pp. 433-437.

[10] H. Padamsee *et al.*, *RF conductivity for accelerators*, Wiley and Sons, New York, 2008.

[11] P. Kneisel *et al.*," Review of ingot niobium as a material for superconducting radio frequency accelerating cavities", *Nucl. Instrum. Methods* A 774, p.133, 2015.

[12] S. K. Chandrasekaran *et al.*, in *Proc. SRF '11*, pp. 593-596.